Progress in Photovoltaics: Research and Applications

WILEY

PROGRESS IN PHOTOVOLTAICS

RESEARCH ARTICLE OPEN ACCESS

Achieving High Efficiencies for Silicon Heterojunction Solar Cells Using Silver-Free Metallization

Mohamed Issifi Yacouba[1] | Andreas Lambertz[1] | Yanxin Liu[1] | Henrike Gattermann[1] | Volker Lauterbach[1] | Karsten Bittkau[1] | Uwe Rau[1,2] | Kaining Ding[1]

[1]IMD-3 Photovoltaics, Forschungszentrum Jülich GmbH, Jülich, Germany | [2]Jülich Aachen Research Alliance (JARA-Energy) and Faculty of Electrical Engineering and Information Technology, RWTH Aachen University, Aachen, Germany

Correspondence: Mohamed Issifi Yacouba (m.issifi.yacouba@fz-juelich.de) | Kaining Ding (k.ding@fz-juelich.de)

Received: 25 September 2024 | **Revised:** 17 June 2025 | **Accepted:** 12 August 2025

Funding: The SHJ Solar Cell and Module Group at the Institute of Energy Materials and Devices–Photovoltaics (IMD-3), Forschungszentrum Jülich, funded and supported this research.

Keywords: copper paste | dispensing | metallization | screen printing | SHJ solar cell | silver-coated copper paste

ABSTRACT

This work investigates the influence of the metallization of low-temperature Cu paste and AgCu paste on the performance of SHJ solar cells through a comprehensive study of two techniques—screen printing (SP) and dispensing. The research successfully applied Cu and AgCu pastes as metal contacts on SHJ solar cells, yielding promising results. Notably, cells with AgCu paste SP on the front side and Ag paste SP on the rear side achieved a 0.13% efficiency gain over reference Ag SP bifacial cells. Moreover, cells with AgCu paste SP on the front side and Cu paste SP on the rear side reached an efficiency of 23.6%, just 0.35% lower than the reference cells, while saving approximately 70% of Ag paste. Cells with Cu paste SP on both sides recorded an average efficiency of 22.4% and a maximum of 23.08%, the highest efficiency reported for cells using Cu SP on both sides (zero Ag). Cells with Cu dispensing on the rear side also demonstrated superior performance compared to cells with Cu SP on the rear side. Along, we assessed the finger-printed characteristics of the three pastes and the performance of SHJ solar cells under various annealing conditions including the Cu annealing conditions (300°C for 5 s). The solar cells maintained stable performance up to 280°C for 5 s, with degradation observed above this temperature, and light soaking partially recovered some of the efficiency loss. A 0.2% drop persisted under Cu annealing conditions, but light soaking reversed this effect back to the original efficiency. This work advances SHJ solar cell technology by highlighting the potential of AgCu and Cu pastes to efficiently replace or reduce Ag paste consumption in SHJ solar cell metallization.

1 | Introduction

Among the silicon-based PV technologies, silicon heterojunction (SHJ) solar cells are attracting a growing interest with a projected market share of 25% by 2030 [1] due to their straightforward processes, high open-circuit voltage, high conversion efficiency, superior passivation, high bifaciality, and low silicon consumption [2, 3]. This technology has achieved a remarkable record power conversion efficiency (PCE) of 27.08% for contacts on both sides [4] and 27.30% for cells with an interdigitated back-contact structure (IBC) [5, 6].

SHJ solar cells are a low-temperature device that has to be processed below 250°C [7]. Due to such temperature constraints, the use of low-temperature Ag paste is important for metal contacts on both cell surfaces. However, low-temperature Ag paste has a relatively higher resistivity than the high-temperature metallization pastes used for passivated emitter and rear cell (PERC)

silicon cells. Therefore, more paste is required to achieve the necessary finger conductivity [8]. Additionally, low-temperature silver paste is the most expensive non-silicon component of a silicon-based solar cell, and its increasing demand makes it a critical factor in cost considerations [9]. Consequently, higher Ag consumption significantly increases the cost of SHJ solar cells [10–12].

Verlinden highlighted that silver consumption for solar cells must be reduced to 5 mg/W or less, or alternative metallization technologies using copper (Cu) must be developed to ensure material sustainability. At a consumption rate of 5 mg/W of silver, achieving a yearly production capacity of 3 TWp—a target set between 2032 and 2050—would consume more than half of the current global annual silver supply [13]. Additionally, according to Zhang et al., to ensure sustainable multi-TW scale production of solar PV within the next decade, long-term silver consumption for solar cells must be restricted to no more than 2 mg/W [14, 15]. If the consumption of Ag is not reduced soon, it will lead to higher costs for solar cells and hinder the sustainable development of the PV industry [16]. Various approaches are being explored to significantly reduce silver consumption in solar cells [17], including:

- First, implementation of fine-line printing by screen printing (SP) process and optimization of screen design [18–20].
- Second, develop alternative printing technologies such as laser pattern transfer printing, rotary screen printing, flex trail printing, and dispenser printing which offer low silver consumption capacity and high aspect ratio [21–24].
- Finally, reducing or replacing Ag with Cu or AgCu is considered due to the abundance and lower cost of Cu [25–28].

Focusing on using Cu paste and/or AgCu paste as an alternative to traditional silver fingers and busbars for metallization in SHJ solar cells offers a promising solution to address Ag scarcity and rising cost challenges [29, 30]. Despite copper's potential to degrade devices due to rapid diffusion into silicon, heterojunction solar cells mitigate this risk as their transparent conductive oxides (TCO) serve as effective diffusion barriers [16, 31–33]. Recently, Cao et al. achieved a certified efficiency of 26.4% by using the electroplating method to prepare Cu electrodes on SHJ cells. Though the impressive photovoltaic performance of Cu electroplating, its complex processes, costly equipment, and environmental concerns pose significant challenges [34–36]. Alternatively, AgCu-based metallization offers a low-cost, environmentally friendly solution, achieving an average efficiency of 25.18% on SHJ solar cells while reducing Ag consumption by 46% compared to traditional Ag electrodes [2]. Similarly, screen-printed Cu paste metallization, replacing most of the Ag in IBC cells as busbars and fingers, delivers comparable performance to IBC cells using Ag paste with an average efficiency of 23%. Notably, no Cu diffusion was observed, even under damp-heat and thermal stress, and Cu fingers remained resistant to oxidation after thermal treatment up to 300°C [16], which is beyond the 250°C process temperature of SHJ solar cells. As a low-temperature manufactured device, SHJ solar cells face challenges with the high-temperature annealing required for Cu metallization, as it can degrade passivation quality, increase recombination losses, and ultimately reduce efficiency [7, 37].

The manufacture of metal contacts for crystalline silicon solar cells is dominated by screen printing because of its efficiency, dependability, and affordability. Nevertheless, contactless methods such as dispenser printing provide accurate, thin, high aspect ratio, uniform lines, increasing productivity and lowering paste consumption. Efficiency gains of up to 2% were reported compared to screen-printed contacts [38]. Dispenser printing reduces silver laydown, and stretching effects plus parallel dispensing further optimize material usage [24, 39]. Despite its advantages, challenges such as nozzle clogging need to be solved. Ongoing research is needed to address these challenges and further develop dispenser printing technology.

In this paper, we investigate the influence of low-temperature Cu paste and AgCu paste (with a weight percentage of ~50 wt% Ag) metallization on the performance of industrial SHJ solar cells through a comprehensive examination of two techniques—screen printing (SP) and dispensing. The aim is to assess the viability of Cu and AgCu pastes as reliable and effective metallization materials for SHJ solar cells, particularly regarding the stability of the SHJ solar cell at the temperatures required for Cu paste annealing. Therefore, we metalized the front and rear sides of the cells with Ag, AgCu, and Cu paste and compared them. Additionally, finger characteristics such as width, height, line resistance, contact resistance, and bulk resistance were evaluated.

2 | Experiments and Methods

To investigate the application of AgCu and Cu pastes on industrial SHJ solar cells compared to reference solar cells utilizing Ag paste, this study employs M2 (244.32 cm^2) solar cells with a wafer thickness of approximately 135 µm (see Figure 1). These solar cells feature a-Si:H (p/i/n) layers, TCO coating, and have no metallization, serving as the starting material for the research. Before considering the metallization of actual solar cells on both sides, the study first examined the performance of screen printed and dispensed fingers from the three different pastes on one side of the wafer. Following this, a preliminary investigation was conducted to assess the impact of various annealing conditions, including those used for Cu metallization, on the performance of industrial SHJ solar cells.

2.1 | Printed-Finger Study

Flatbed screen printing (SP) was used for printing Ag and AgCu fingers with a knotless screen featuring a 23-µm finger opening, 430 wires per inch, a wire diameter of 13 µm, and an emulsion thickness of 8 µm. For the higher viscosity Cu paste (500 Pa·s vs. 250 Pa·s for Ag), a 30-µm finger opening screen was used with 430 wires per inch, a wire diameter of 13 µm, and an emulsion thickness of 19 µm. The same screen design was utilized for all three pastes, incorporating 96 fingers with a pitch of 1.6 mm. Additionally, single-nozzle dispensing was employed to print Ag, AgCu, and Cu pastes. Specific printing parameters, such as squeegee speed, snap-off distance, and flat-bed speed, were adjusted for each paste type, with separate dispensing parameters tailored to accommodate the distinct properties of each paste. This setup enabled

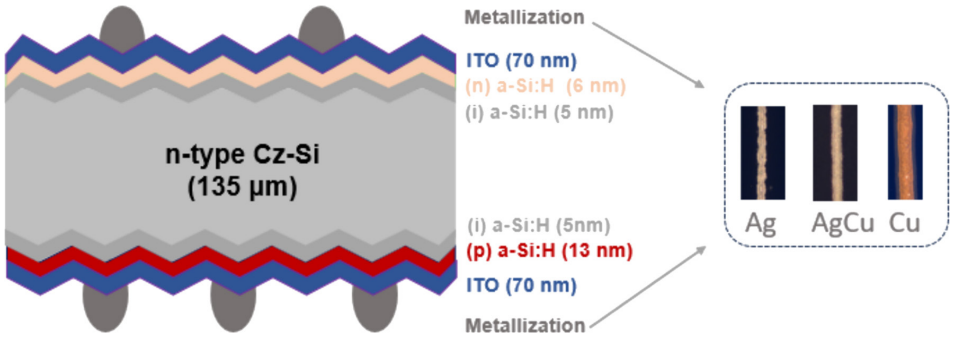

FIGURE 1 | The schematic structure of a bifacial SHJ solar cell used in this study with different metallization pastes (not to scale).

a comparative analysis of the printability performance of the different pastes. After printing, the lines were dried at 150°C for 10 min for Ag and AgCu pastes and at 100°C for 2 min for Cu paste. Subsequently, the fingers were annealed at 170°C for 40 min for Ag and AgCu and at 300°C for 5 s for Cu as recommended by the paste manufacturers. The Ag and AgCu fingers were annealed using an oven, while the Cu fingers annealing was done using a manual process that places the solar cells on a hot plate.

Due to Cu's sensitivity to oxidation, especially during annealing, Cu lines were annealed under a protective cover (e.g., backing paper) to prevent contact with atmospheric oxygen [26, 27]. Additionally, as we typically employ double printing for front-side SP, the drying process is usually carried out after the first printing before applying the second printing, or after printing one side before moving on to print the other side. For Cu fingers, drying is also performed prior to wrapping the cells with Cu fingers in the protective cover for annealing.

Here, we aim to figure out information about the electrical performance and geometry for the aforementioned pastes. The investigation included examining the geometry (width, height, and cross-section) of the metal fingers (Ag, AgCu, Cu) using a Zeta 3D microscope and a laser scanning confocal microscope. Following this, the line resistance was measured and calculated using the four-probe method after annealing the samples under the specified conditions. The contact resistivity of metals to TCO in final SHJ solar cells was also measured via the transmission line method (TLM), which utilizes variable distanced pads of 2 mm width and 10 mm length [40, 41]. Subsequently, the fingers bulk resistance was calculated. The weight of the fingers was measured using a precise electronic balance [42] with an accuracy of 0.1 mg.

2.2 | Impact of Annealing on SHJ Solar Cell's Performance

SHJ solar cell devices are manufactured below 250°C [7]. In contrast, the standard annealing conditions for Cu paste metallization are 300°C for 5 s. Therefore, before applying standard Cu metallization annealing conditions to SHJ solar cells, an investigation was conducted on externally Ag screen-printed SHJ solar cells with busbars to evaluate the potential effects of different annealing conditions, including those used for Cu metallization, on their performance. This investigation involved using three cells for each of the following annealing conditions:

- For 5 s of annealing, temperatures of 280°C, 320°C, and 360°C were tested.
- For 300°C, durations of 5, 20, and 40 s were tested.

After each annealing condition, light soaking was performed on the cells to evaluate if any efficiency losses observed could be recovered. For this experiment, fast light soaking was made on the characterized solar cells (~90 s). During the process, the solar cells were exposed to an LED-based light source with an input intensity of 55 kW/m^2 at about 175°C [43].

2.3 | Application of the Pastes on SHJ Solar Cells and Characterization

After studying the finger performance of the three pastes and investigating the impact of various annealing conditions, including the standard annealing conditions for Cu paste on industrial SHJ solar cells, we proceeded to apply those pastes (Ag, AgCu, Cu) on metallization-free industrial SHJ solar cells coated with TCO to assess their influence on the performance of SHJ solar cells (see Figure 1). These metallization-free cells were selected for their similarity to our in-house SHJ solar cells. They were chosen to simplify the study. In this experiment, the pastes and printing tools for metallization were varied for both the front and rear sides.

For the front-side metallization with Ag, AgCu, and Cu pastes, the SP fingers were done using the same screens used for finger-printed study (in Section 2.1). For the rear-side metallization, only Cu and Ag were considered and compared. A screen with a finger opening of 60 µm, 350 wires per inch, a wire diameter of 16 µm, and an emulsion thickness of 9 µm was used for the rear-side screen printing of all pastes. This screen design incorporated 250 fingers with a pitch of 0.9 mm. Additionally, single-nozzle dispensing was employed for Cu rear-side metallization. Due to the wider finger dimensions, this approach necessitated a modification, with only 96 fingers dispensed on the rear side while maintaining a pitch of 1.6 mm. Notably, metallization on both sides of the cells was carried out without busbars.

AgCu paste application has already been investigated in previous research [2, 23], and it is mainly used here for comparison

with Ag and Cu. In SHJ solar cells, front-side metallization is more critical than rear-side metallization due to the trade-off between optical shading and electrical performance, which affects the overall cell efficiency, short-circuit current density J_{sc}, fill factor *FF*, and series resistance R_s [44]. Therefore, this work primarily focused on the front-side metallization by applying and comparing the performance of the three pastes Ag, AgCu, and Cu. For rear-side metallization, only Cu paste with Ag paste was considered and compared.

After printing, the annealing of the metallized fingers (for the different pastes) was performed as described in Section 2.1. However, light soaking (LiSo) was not performed on these metallized solar cells because the Cu fingers cannot currently be adequately protected from oxidation at the 175°C LS temperature. Methods like protective wrapping are being explored to enable LiSo for Cu cells. The electrical characteristics, including IV parameters and electroluminescence (EL) measurements of the solar cells were then assessed using the LOANA system from pv-tools with a Wavelabs LED light source (Sinus 220) under standard test conditions (STC: AM1.5 G, 25°C, 1000 W/m^2). A 12-contact bar frame was used for front-side contact, which has a voltage sense of approximately 25% between contact bars. This means that finger line resistance is not accounted for during IV measurement [45]. Back-side contact of the cells is performed using a fully conductive chuck. Therefore, the effect of rear-side line resistance is negligible. The EL measurements of the cells were conducted with a high injection current of 8 A to capture detailed EL images.

3 | Results and Discussion

3.1 | Analysis of the Printed Fingers

This study aims to investigate the electrical performance and geometry of fingers for all pastes. Figure 2 presents the finger patterns and widths measured with a confocal microscope for the three pastes, while Figure 3 illustrates the measured and calculated line resistance as a function of finger width. Additionally, Table 1 presents the average data for measured finger widths, height aspect ratio, line resistance, contact resistivity, bulk resistance, and Ag weight.

Figure 2 shows the finger shapes produced by SP and dispensing methods in our laboratory using Ag paste, AgCu paste, and Cu paste. Due to limitations of the dispenser such as nozzle clogging, the dispensing method results in wider, yet more homogeneous and continuous fingers compared to screen printing, making it suitable for rear-side applications [16] and potentially improving electrical contact performance. Using the same screen type, AgCu SP fingers produce almost similar average line widths compared to Ag SP, while Cu SP fingers are wider than both Ag and AgCu SP fingers, which is due to the use of a wider screen opening for Cu. However, the finger geometry of Cu SP in our study is similar to the Cu fingers reported by Teo et al. [46] and finer than those in previous reports with Chen et al. [16].

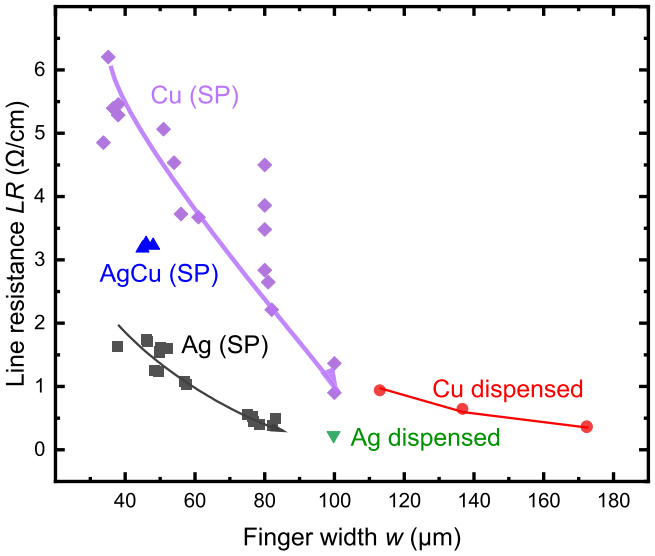

FIGURE 3 | Line resistance (LR) as function of finger width (w) of metal fingers for Ag SP in grey, Ag dispensed in green, AgCu SP in blue, Cu SP in purple, and Cu dispensed in red.

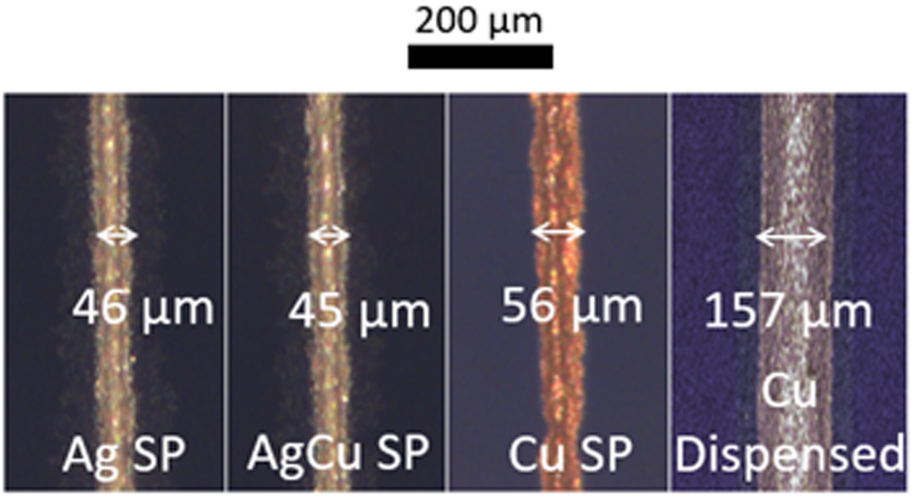

FIGURE 2 | Microscopy images of (a) Ag SP finger, (b) AgCu SP finger, (c) Cu SP finger, and (d) Cu dispensed finger.

TABLE 1 | Electrical performance and geometry of Ag, AgCu, and Cu fingers.

Finger	Width (W, μm)	Height (H, μm)	Aspect ratio (H/W)	Line resistance (Ω/cm)	Contact resistivity (mΩ*cm^2)	Bulk resistance (10^{-6} Ω*cm)	Ag weight (mg)
Ag SP	46.56	14.21	0.30	1.15	5.04	3.51	35.45
Cu SP	56.18	10.22	0.18	4.24	10.28	12.62	0.00
Cu dispensed	152.98	34.51	0.22	0.90	[a]	1.68	0.00
AgCu SP	45.26	12.55	0.27	3.20	8.10	7.20	16.80

Note: These results are the mean values and concern only the front-side screen printed fingers and dispensed Cu fingers.
[a]Not measured.

Figure 3 shows the line resistance versus finger width for various pastes and printing techniques. The legend, defined by color, indicates the line resistance for fingers made by Ag SP in grey, Ag dispensing in green, Cu SP in purple, Cu dispensing in red, and AgCu SP in blue, plotted as a function of their respective finger widths. A consistent pattern emerges, indicating a decline in finger line resistance with increasing finger width across all pastes and printing methods examined. Additionally, both Cu dispensing and Cu SP typically exhibit higher average line resistance compared to Ag SP when extrapolating the finger width of Ag SP to have the same width as Cu printed lines. Specifically, fingers from Cu screen printing show approximately three times the average line resistance of fingers from Ag SP (3.6 Ω/cm compared to 1 Ω/cm for a 60 μm finger width). Furthermore, AgCu fingers demonstrate higher line resistance compared to pure Ag fingers (3.2 Ω/cm compared to 1.8 Ω/cm for a finger width of around 40 μm), yet lower than that of Cu. By extrapolating the trend from Ag SP fingers line resistance data, it reveals that Ag dispensed fingers have similar line resistance to Ag SP fingers, and Cu dispensing still presents higher line resistance compared to Ag SP and dispensed fingers. Therefore, the homogeneity of dispensed lines does not appear to impact significantly the line resistance. The large distribution in Cu SP finger line resistance for a constant finger width can be attributed to a slight variation during the annealing process. While the standard conditions are 300°C for 5 s, the process still involves some manual steps, making it challenging to ensure precise timing for all samples. Table 1 presents the average finger line characteristics for the three types of paste, including finger width, height, aspect ratio, line resistance, contact resistivity, bulk resistance, and Ag weight. For all the pastes, the front-side printing fingers and Cu dispensing were considered for the measurements of finger width, height, aspect ratio, bulk resistance, Ag weight, and line resistance. In Table 1, Ag fingers serve as the reference, and the data for the other two pastes are compared to that of Ag fingers.

Table 1 shows that, despite using a wider opening screen for Cu, compared to Ag and AgCu, Cu fingers exhibit higher line resistance, contact resistivity, and bulk resistance, approximately 4.24 Ω/cm, 10.28 mΩ*cm^2, and 12.62×10^{-6} Ωcm, respectively. Evidently, the wider screen opening has resulted in wider fingers and a lower aspect ratio. Cu-dispensed lines, as previously noted, are currently wider but exhibit more homogeneous line features compared to SP lines; hence, it is used only for the rear side. These characteristics provide lower line resistance and volume resistance for dispensed Cu lines. Furthermore, AgCu paste fingers exhibits higher line resistance, bulk resistance, and contact resistivity than the pure Ag paste due to the presence of Cu and other factors such as printability, and finger morphology, which might include rheological behavior, aggregation, dispersion, and particle distribution, among other things. Additionally, due to the unoptimized screen printing process on the rear side, this analysis only considers the Ag weight from the front-side metallization and Cu dispensing. The results show an Ag weight of 35.45 mg when using pure Ag paste SP, whereas an Ag weight of 16.80 mg is achieved with the AgCu paste SP. This reduction of the Ag content is due to the AgCu paste containing 50% less silver, with the remaining metal content being replaced by Cu. In contrast, using only Cu (via screen printing or dispensing) for metallization results in zero Ag weight.

The use of Cu and/or AgCu as an alternative to Ag in solar cells can reduce dependency on the expensive and scarce Ag. However, their significantly higher line resistance and bulk resistance pose challenges for their application. AgCu paste, which contains approximately 50% Cu particles, results in an estimated 50% reduction in Ag consumption when applied to SHJ solar cells while still maintaining high efficiency in solar cells [2].

3.2 | Solar Cell Results and Discussion

This section presents the analysis and discussion of the solar cells IV parameters results and some electroluminescence (EL) images. It is structured into two parts. First, it addresses the investigations on the impact of annealing conditions on the performance of SHJ solar cells. Second, it examines the applications of different pastes on SHJ solar cells.

Figure 4 shows the efficiency of solar cells versus the annealing conditions on solar cells. For each annealing condition, we have the cells' performance for before sintering (bS), after sintering (aS), and light-soaked (LiSo). Figure 4a shows the efficiency versus different sintering temperatures, each for 5 s. Figure 4b plots efficiency against different sintering times at 300°C.

Figure 4a indicates a gradual decrease in solar cell performance with increasing annealing temperature, with some recovery after light soaking, except for the 280°C annealing temperature,

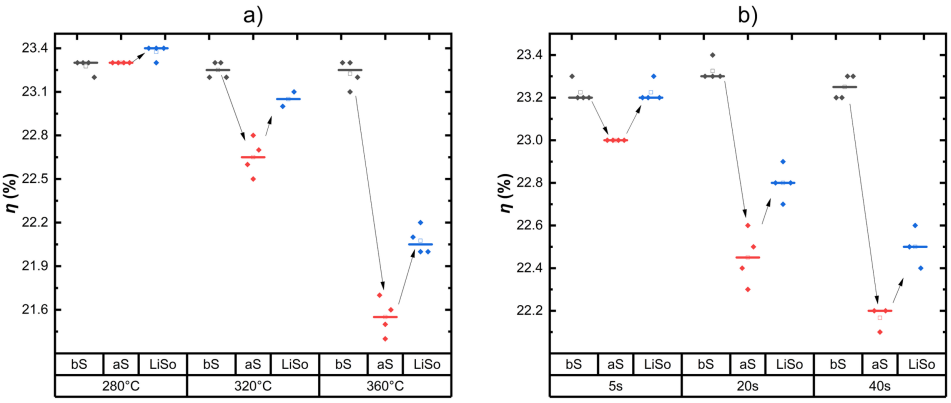

FIGURE 4 | (a) Efficiency for SHJ solar cells before sintering (bS), after sintering (aS) at different temperatures (280°C, 320°C, and 360°C) for 5 s and light soaked (LiSo). (b) Efficiency for SHJ solar cells before sintering (bS), after sintering (aS) for different sintering times (5, 20, and 40 s) at 300°C and light soaked (LiSo) for different batches of SHJ solar cells with Ag fingers and busbars.

which actually resulted in an improvement in efficiency after light soaking. Treatments at 320°C and 360°C resulted in a decrease in efficiency of about $0.5\%_{abs}$ and $1.5\%_{abs}$, respectively. These reductions are likely due to the partial escape of hydrogen atoms from the passivation film, thus increasing the dangling bond density in the amorphous layer and at the a-Si:H/c-Si interface [47]. Slight efficiency improvements were observed in these treated cells after light soaking, consistent with previous reports [48], which are attributed to their improved open-circuit voltage V_{oc} and fill factor *FF* (see Figure A1).

Similarly, solar cells treated at different sintering times at 300°C showed similar effects, as shown in Figure 4b. There was a decrease in efficiency of about $0.2\%_{abs}$ for a 5-s sintering time at 300°C, the standard condition for annealing Cu pastes, but light soaking reversed this effect back to the original efficiency. Beyond this condition, irreversible performance degradation is evident. IV (or photovoltaics) parameters explaining this efficiency variation are provided in Figure A2.

Subsequently, we analyze the results of applying various pastes to SHJ solar cells with different metallization combinations. Precisely, cells with Cu on the rear side were combined with Cu, AgCu, and Ag on the front side. Similarly, cells with Ag on the rear side were combined with Cu, AgCu, and Ag on the front side. In Figure 5, the IV (or photovoltaics) parameters are organized such that the front-side metallization is shown in the first (upper) row, and the rear-side metallization is shown in the second (lower) row. Notably, due to the inability to achieve fine dispensed lines with the current setup and pastes, dispensing is used for Cu paste and only on the rear side.

Figure 5 shows the measured *IV* parameters of solar cells with various front and rear side metallizations applying both screen printing (SP) and dispensing as printing tools. The results of some special champion cells are presented in Table 2.

In each graph, the first set of solar cells has Ag SP on the rear side and Ag SP, AgCu SP, and Cu on the front side. The second set has Cu SP on the rear side and Ag SP, AgCu SP, and Cu SP on the front side. The final set has Ag SP on the front side and Cu dispensed on the rear side. This structure was selected for the reasons previously outlined regarding the significance of front-side metallization.

3.2.1 | Variation of the Rear-Side Metallization

From Figure 5, we first analyze the effect of rear-side paste application and variations, while keeping the front side constant. As highlighted in Figure 5a, taking Ag SP on the rear side as a reference, we observe a decrease in efficiency with Cu SP on the rear side, regardless of the front side paste. Cells with Cu dispensed on the rear side also show a decrease in efficiency compared to Ag SP rear side cells, but this decrease is less pronounced than for cells with Cu SP rear side, highlighting the potential advantage of paste dispensing as reported in the GECKO project [38].

Including the absolute efficiency loss of $0.2\%_{abs}$ for cells with Cu due to annealing conditions, the average efficiency of cells with Cu SP on the rear side is 22.7%, 23.35%, and 22.4% when combined with Ag SP, AgCu SP, and Cu SP on the front side, respectively. In comparison, cells with Ag SP on the rear side have an average efficiency of 23.7%, 23.9%, and 22.6% with Ag SP, AgCu SP, and Cu SP on the front side, respectively. Cells with Cu dispensed on the rear side and Ag SP on the front side show an average efficiency of $22.96\%_{abs}$. This corresponds to a drop in efficiency for cells with Cu SP on the rear side compared to Ag SP as follows: $1\%_{abs}$ (Ag SP front), $0.55\%_{abs}$ (AgCu SP front), and $0.2\%_{abs}$ (Cu SP front) as indicated by grey, red, and blue arrows, respectively. This indicates that the efficiency drop for cells with Cu rear side is more pronounced when there is Ag SP on the front side, then with AgCu SP on front side, and lastly with Cu SP front. For cells with Cu dispensed on the rear side and Ag SP on the front, the efficiency drop is about $0.74\%_{abs}$ (grey dashed arrows) compared to cells with Ag SP on the rear side.

These results highlight the impact of using Cu (both SP and dispensed) on the front side, rear side, or both sides of SHJ solar cells, particularly the impact of the Cu annealing conditions. Compared to cells with Ag on the rear side, those with Cu exhibit reduced efficiency, attributed to a lower fill factor

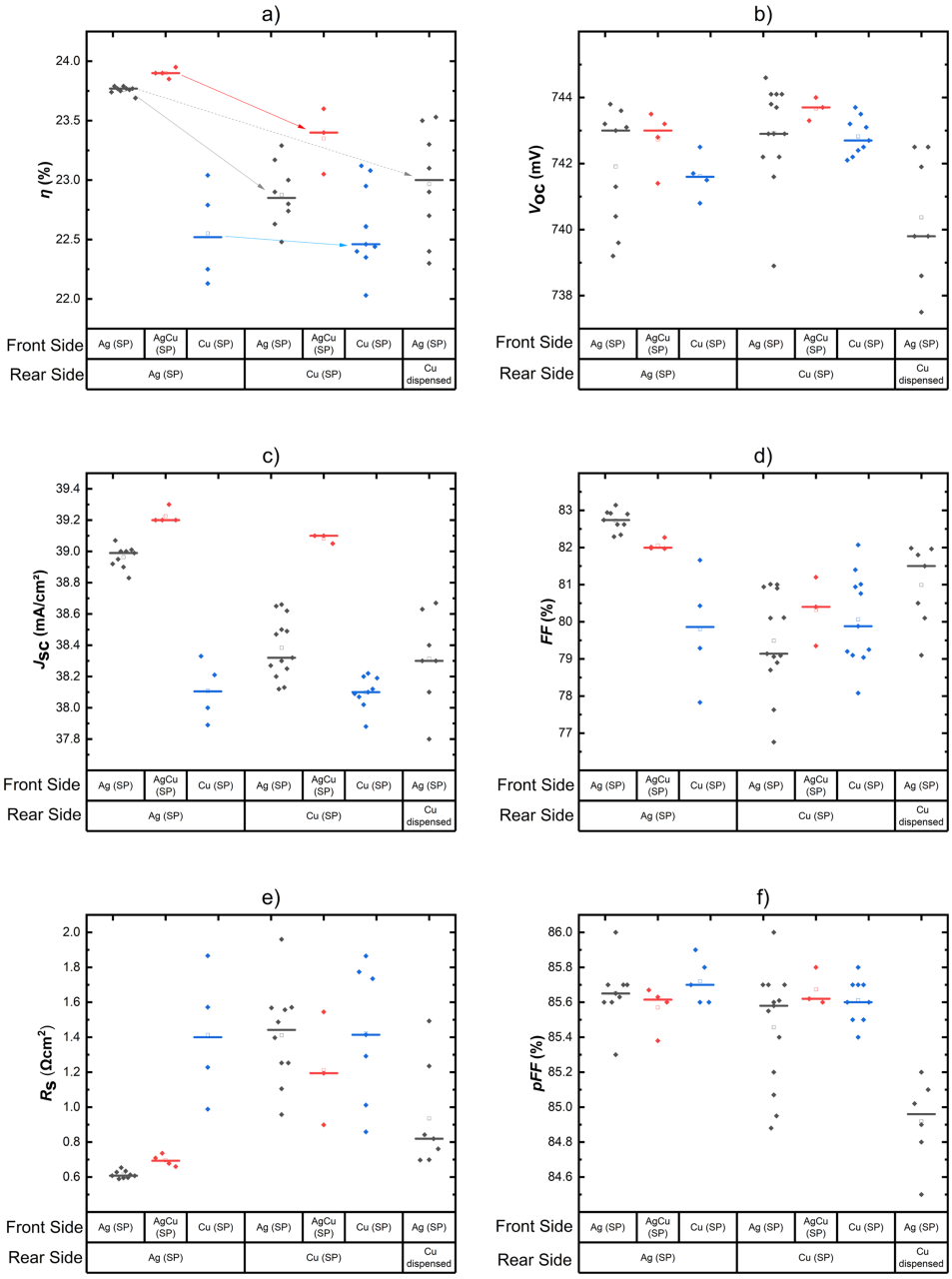

FIGURE 5 | Photovoltaics parameters showing (a) the efficiencies (η), (b) the open-circuit voltages (V_{oc}), (c) the short-circuit current densities (J_{sc}), (d) the fill factors (FF), (e) the series resistances (R_s), and (f) the pseudo-fill factors (pFF), of solar cells with various front and rear side metallizations applying both screen printing (SP) and dispensing as printing tools. The parameters are organized such that the front-side metallization is shown in the first (upper) row, and the rear-side metallization is shown in the second (lower) row.

TABLE 2 | IV-summary of some champion cells with a reduction of Ag usage.

Cells	Ag reduction (%)	η (%)	J_{sc} (mA/cm²)	V_{oc} (mV)	R_s (Ωcm²)	*FF* (%)	*pFF* (%)
Ag bifacial (reference)	00	23.79	38.94	739.60	0.59	82.62	85.60
AgCu front/Ag rear	25	23.95	39.16	743.50	0.66	82.27	85.70
AgCu front/Cu rear	70	23.62	39.13	743.30	0.91	81.20	85.60
Cu bifacial	100	23.08	37.88	742.40	0.85	82.07	85.70

(*FF*) with an average decrease of 0.5% to 3%. This *FF* reduction is associated with higher R_s, as illustrated in Figure 5d,e. Notably, cells with Ag SP on the front side and Cu dispensed on the rear side show a 0.53% absolute increase in efficiency compared to cells with Ag SP on the front side and Cu SP on the rear side.

3.2.2 | Variation of the Front-Side Metallization

Now, we analyze the results of paste variations on the front side for each type of rear-side paste application (Ag and Cu). Front-side metallization was done with Ag SP (grey), AgCu SP (red), and Cu SP (blue). Considering the average efficiency of all the cells with Ag SP on the rear side, we observed an increase in efficiency of $0.2\%_{abs}$ for AgCu on the front side and a decrease in efficiency of $1.1\%_{abs}$ for Cu on the front side with respect to Ag on the front side. For cells with Cu SP on the rear side, we observed an increase in efficiency of $0.65\%_{abs}$ for AgCu on the front side and a decrease in efficiency of $0.3\%_{abs}$ for Cu on the front side compared to Ag on the front side.

The $0.2\%_{abs}$ efficiency increase for the AgCu front side contrasts with previous results [1], which reported a $0.13\%_{abs}$ decrease in efficiency for AgCu on the front side. This increase in efficiency is even more pronounced ($0.85\%_{abs}$) for cells with Cu on the rear side, leading to the following observation: Although AgCu SP exhibits higher bulk resistance and contact resistivity compared to Ag SP, its application in solar cells front side metallization results in higher efficiency due to its resulting higher J_{sc} and V_{oc}. Notably, cells with AgCu SP on the front side and Cu SP on the rear side show impressive performance, achieving up to $23.6\%_{abs}$ efficiency with minimal Ag usage. This represents only a $0.35\%_{abs}$ decline in efficiency compared to bifacial Ag cells while offering approximately 70% savings in Ag consumption due to the Cu content in the AgCu paste.

Another important result is that despite their lower J_{sc}, *FF*, and higher R_s (see Figure 5c–e), cells with Cu SP on both sides (zero Ag) achieve an outstanding average efficiency of $22.4\%_{abs}$ and a champion cell's efficiency of $23.08\%_{abs}$. Furthermore, cells with one side (front or rear) Cu application with Ag at the opposite side show as well remarkable performance. To our knowledge, this result is the highest efficiency of a SHJ solar cell achieved using Cu SP (without Ag) on both sides.

To provide further insights into the causes of the observed efficiency variations in the cells, Figure 5 presents further IV parameters: Figure 5b shows the open-circuit voltage (V_{oc}) of the cell batches. It shows a similar range of V_{oc} across all solar cell batches, with cells having Cu dispensed on the rear side showing slightly lower Voc. In addition, Figure 5c illustrates the short-circuit current density (J_{sc}) of the cell batches. This graph shows a slightly higher J_{sc} for cells with AgCu front compared to cells with Ag front and much lower J_{sc} for cells with Cu finger on the front side. Given that the average difference in finger width is only 1 μm between Ag and AgCu and 10 μm between Ag and Cu (see Table 1), the slightly higher J_{sc} of cells with AgCu front compared to cells with Ag front can only be slightly attributed to the finer AgCu fingers, and the lower J_{sc} for cells with Cu finger on the front side can be partly attributed to the wider fingers. Further analysis and additional experiments are necessary and currently underway to fully understand the underlying mechanisms driving this behavior. As suggested by Siraj et al., this increase might also result from an improvement in optical reflectance [49]. Additionally, as expected, cells with a Cu-dispensed rear side show similar J_{sc} to those with a Cu SP rear side but exhibit lower V_{oc} performance compared to Cu SP rear side, all having an Ag SP front side. Therefore, the higher efficiency of cells with Cu-dispensing rear side compared to those with Cu SP rear side is attributed to their lower contact resistance due to the higher metal coverage of the Cu dispensed lines on the backside brought by the wider fingers in combination with the more homogeneous features, thus resulting in a lower series resistance (R_s) and higher fill factor (*FF*). The fill factor (FF) of cell batches is illustrated in Figure 5d, which shows a lower FF compared to all the reference solar cells. In general, cells with at least one side Cu metallization show low FF, and the data are scattered in the same range, making direct comparisons challenging. Cells with AgCu SP pattern is consistent with some previous data [2], where the AgCu front side results in slightly higher R_s and lower FF compared to Ag for cells with Ag rear side. As previously mentioned, the higher average FF for cells with Cu dispensed on rear side compared to cells with Cu SP on the rear is due to metallization design and the higher metal coverage of the Cu dispensed lines on the backside brought by the wider fingers in combination with the more homogeneous features. This trend in FF inversely correlates with the variation in R_s, which displays the opposite pattern. In Figure 5e, the R_s data show an increase from Ag front to AgCu front, and then to Cu front for cells with Ag rear side metallization. Similarly to FF, cells with Cu metallization present scattered R_s data. Nonetheless, the R_s increase is less pronounced for cells with rear-side Cu dispensing, therefore displaying higher FF compared to cells with rear-side Cu SP. Since our IV tester does not take into account the line resistance effect of the fingers, the higher R_s observed may be brought by the higher contact resistivity of AgCu and Cu respectively, which is worsened by the larger number of fingers, especially for both sides of Cu metallization cells (96 fingers on the front and 250 fingers on the rear side). Additionally, scanning electron microscopy (SEM) was used to analyze the microstructural changes of SP Cu paste at various stages of curing. This analysis revealed unsintered Cu nanoparticle regions and areas where Cu nanoparticles exhibited poor contact with each other and with ITO, even after sintering at 300°C. This is a possible reason for a higher contact resistivity of fingers with TCO, reducing efficiency of electron transfer during conduction, therefore contributing to an increase in the R_s [46].

The pseudo-fill factor (pFF) results for all cells are plotted in Figure 5f. The data show approximately similar average pFF values for all cell types, except for cells with Cu dispensed on the rear side, which exhibited a lower pFF of approximately $0.6\%_{abs}$. This slight reduction of pFF and Voc observed in cells with Cu dispensed on the rear suggests the absence of diffusion of Cu. Chen et al. reported that, if significant Cu diffusion into silicon had occurred, it would have led to a much greater degradation in pFF and Voc [16]. This slight decrease in pFF and Voc could be attributed to minor cell damage caused by handling during the dispensing process, which involves more manual steps compared to SP. Despite the differences in performance observed for all the types of cells, cells with at least one side Cu, in particular, exhibit scattered data for all the other IV parameters. This scattering is caused by the inherent variability of the Cu annealing process in timing across samples, making it more challenging to achieve stable

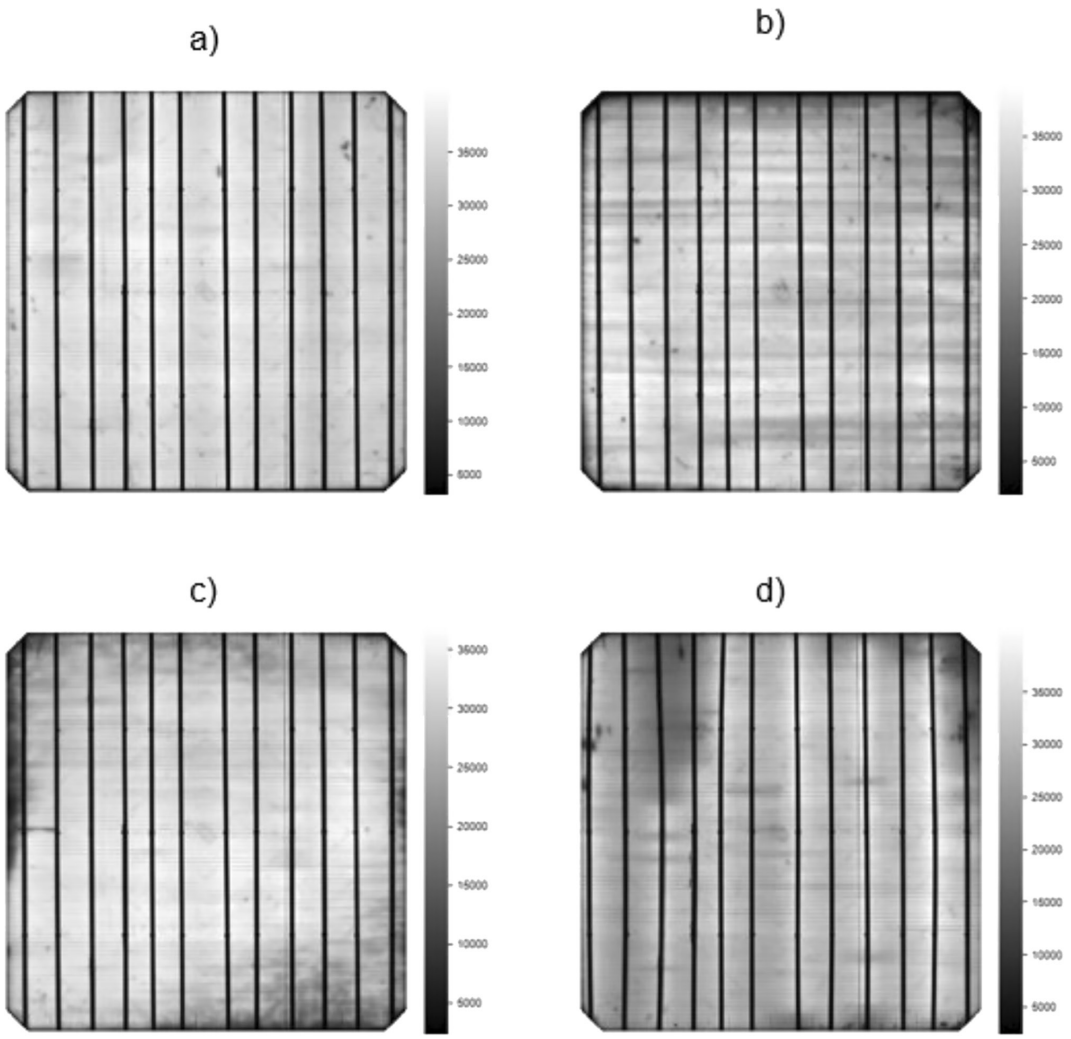

FIGURE 6 | (a) EL image for the reference solar cells, (b) EL image for solar cells with Cu SP front side and Ag SP rear side, (c) EL image for solar cells with Ag SP front side and Cu SP rear side, and (d) EL image solar cells with both sides SP Cu, each under high current injection of 8 A (32.74 mA/cm^2).

performance. In addition, this scattering indicates the need to optimize the Cu printing and annealing processes. A summary of the IV results for the champion cells is provided in Table 2.

Figure 6 shows electroluminescence (EL) images of some SHJ solar cells metallized with Cu SP, compared to reference cells with Ag SP on both sides. The EL images reveal dark areas on all Cu-metalized cells, particularly at the edges. This darkening indicate potential contact issues between the Cu fingers and the TCO, likely due to poorly sintered regions as reported Teo et al. [46], which is especially problematic for cells with Cu on both sides (see Figure 6d). Addressing these Cu contact issues could potentially resolve the problem and improve the efficiency in a more stable manner. However, the bent appearance of the test line in Figure 6d results from a slight misalignment of the current bar in the IV testing frame. This misalignment leads to uneven current distribution during EL imaging. These features do not reflect actual defects in the solar cell structure.

4 | Conclusion

In this work, the influence of metallization with Cu paste and AgCu paste on SHJ solar cells was investigated through screen printing and dispensing, and their performance was compared to that of the reference cells with Ag on both sides. Initially, we compared the line resistance, finger width, aspect ratio, contact resistivity, and bulk resistance of AgCu, Cu, and Ag pastes. This comparison revealed that Cu exhibited higher performance metrics than AgCu, which in turn outperformed Ag. Investigation of SHJ solar cells under different annealing conditions revealed a degradation threshold at temperatures exceeding 280°C for 5 s, but recovery can be achieved through light-soaking techniques. This results in 0.2%$_{abs}$ efficiency drop of SHJ solar cells under Cu annealing conditions (300°C, 5 s). SHJ solar cells with screen-printed (SP) AgCu paste on the front and Ag paste on the rear side achieved an average efficiency improvement of +0.13% absolute compared to reference Ag SP bifacial cells. Cells with SP AgCu on the front and SP Cu on the rear side reached an efficiency of up to 23.6% absolute, only 0.35% lower than reference

cells, while saving approximately 70% of Ag paste. Notably, cells with SP Cu on both sides achieved an average efficiency of 22.4% absolute and a maximum of 23.08% absolute, representing the highest performance recorded for cells with Cu SP on both sides (zero Ag). Furthermore, Cu dispensing on the rear side demonstrated better performance than Cu SP. To maximize the potential of AgCu and Cu pastes, it is essential to optimize and standardize Cu screen printing and dispensing processes, reduce dispensed finger widths, and conduct further research on printing processes, stability, reliability, and economic benefits. The findings demonstrated that SHJ solar cells with silver-free metallization on both sides achieved efficiencies above 23%, indicating that the target of 2 mg/W of Ag consumption per cell is feasible with high-efficiency SHJ solar cells.

Author Contributions

Mohamed Issifi Yacouba and Andreas Lambertz: Conceptualization of the study. Experiments and characterization: Mohamed Issifi Yacouba, Yanxin Liu, Henrike Gattermann, and Volker Lauterbach. Data analysis: Mohamed Issifi Yacouba, Andreas Lambertz, Yanxin Liu, Henrike Gattermann, Volker Lauterbach, Karsten Bittkau, Kaining Ding, and Uwe Rau. Mohamed Issifi Yacouba wrote the original draft. Study supervision: Andreas Lambertz, Kaining Ding, and Uwe Rau. All authors read and approved the final version.

Acknowledgments

We sincerely thank the SHJ Solar Cell and Module Group at the Institute of Energy Materials and Devices–Photovoltaics (IMD-3), Forschungszentrum Jülich, for their funding and support of this research. Our gratitude also extends to Wilfried Reetz, Gunnar Schöpe, and the entire institute staff for their invaluable assistance and resources, which significantly contributed to this work. Additionally, we acknowledge the support from the European projects Nordstrom, EMPower, and SiLEAN and the Energy and Green Hydrogen program under WASCAL. We also appreciate the valuable contributions from the COPRRINT team. Lastly, we would like to thank the reviewers for their insightful comments throughout the review process. Open Access funding enabled and organized by Projekt DEAL.

The authors used DeepL and Chat GPT to enhance the text's readability when preparing this article. The writers took full responsibility for the publication's content after using this tool, reviewing and editing it as necessary.

Conflicts of Interest

The authors declare no conflicts of interest.

Data Availability Statement

The data that support the findings of this study are available from the corresponding author upon reasonable request.

References

1. "International Technology Roadmap for Photovoltaic_itrpv_results_14th Edition_2023," 2023.

2. D. Du, H. Huang, X. Li, et al., "Low-Cost Metallization Based on Ag/Cu Fingers for Exceeding 25% Efficiency in Industrial Silicon Heterojunction Solar Cells," *Solar RRL* 8 (2024): 2400052, https://doi.org/10.1002/solr.202400052.

3. Y. Zeng, C. W. Peng, W. Hong, et al., "Review on Metallization Approaches for High-Efficiency Silicon Heterojunction Solar Cells," *Transactions of Tianjin University* 28 (2022): 358–373, https://doi.org/10.1007/s12209-022-00336-9.

4. "Trina Solar Hits New 27.08% Record for HJT Solar Cell," pv Magazine International, accessed Feb 23, 2025, https://www.pv-magazine.com/2024/12/19/trina-solar-hits-new-27-08-record-for-hjt-solar-cell/.

5. LONGi, "LONGi Sets a New World Record of 27.09% for the Efficiency of Silicon Heterojunction Back-Contact (HBC) Solar Cells," LONGi News, accessed Mar 2, 2024, https://www.longi.com/en/news/heterojunction-back-contact-battery/.

6. "LONGi Unveils HBC Cell With Record 27.3% Conversion Efficiency," PVTECH, accessed May 22, 2024, https://www.pv-tech.org/longi-heterojunction-back-contact-cell-27-3-conversion-efficiency/.

7. D. Chen, L. Zhao, H. Diao, W. Zhang, G. Wang, and W. Wang, "Choice of the Low-Temperature Sintering Ag Paste for a-Si:H/c-Si Heterojunction Solar Cell Based on Characterizing the Electrical Performance," *Journal of Alloys and Compounds* 618 (2015): 357–365, https://doi.org/10.1016/j.jallcom.2014.08.175.

8. M. Taguchi, A. Yano, S. Tohoda, et al., "24.7% Record Efficiency HIT Solar Cell on Thin Silicon Wafer," *IEEE Journal of Photovoltaics* 4, no. 1 (2014): 96–99, https://doi.org/10.1109/JPHOTOV.2013.2282737.

9. N. Amin, S. Santhiran, N. M. Kassim, A. A. Alkahtani, M. A. Islam, and M. Y. Mohd Yusof, "Impact Analysis of Metallization Design and Recombination Losses on Performance of Crystalline Silicon Solar Cells," *Energies* 16, no. 18 (2023): 6505, https://doi.org/10.3390/en16186505.

10. A. Razzaq, T. G. Allen, W. Liu, Z. Liu, and S. De Wolf, "Silicon Heterojunction Solar Cells: Techno-Economic Assessment and Opportunities," *Joule* 6 (2022): 514–542, https://doi.org/10.1016/j.joule.2022.02.009.

11. K. Yoshikawa, W. Yoshida, T. Irie, et al., "Exceeding Conversion Efficiency of 26% by Heterojunction Interdigitated Back Contact Solar Cell With Thin Film Si Technology," *Solar Energy Materials and Solar Cells* 173 (2017): 37–42, https://doi.org/10.1016/j.solmat.2017.06.024.

12. S. DeWolf, A. Descoeudres, Z. C. Holman, and C. Ballif, "High-Efficiency Silicon Heterojunction Solar Cells: A Review," *Green* 2 (2012): 7–24, https://doi.org/10.1515/green-2011-0018.

13. P. J. Verlinden, "Future Challenges for Photovoltaic Manufacturing at the Terawatt Level," *Journal of Renewable and Sustainable Energy* 12, no. 5 (2020): 053505, https://doi.org/10.1063/5.0020380.

14. Y. Zhang, M. Kim, L. Wang, P. Verlinden, and B. Hallam, "Design Considerations for Multi-Terawatt Scale Manufacturing of Existing and Future Photovoltaic Technologies: Challenges and Opportunities Related to Silver, Indium and Bismuth Consumption," *Energy & Environmental Science* 14, no. 11 (2021): 5587–5610, https://doi.org/10.1039/d1ee01814k.

15. M. Kim, L. Wang, Y. Zhang, R. Underwood, S. Drury, and B. Hallam, "Roadmap Towards Sustainable SHJ Solar Cell Design," in *AIP Conference Proceedings* (AIP Publishing, 2023): 2826, https://doi.org/10.1063/5.0140906.

16. N. Chen, D. Rudolph, C. Peter, et al., "Thermal Stable High Efficiency Copper Screen Printed Back Contact Solar Cells," *RRL Solar* 7, no. 2 (2023): 2200874.

17. S. Pingel, T. Wenzel, N. Göttlicher, et al., "Progress on the Reduction of Silver Consumption in Metallization of Silicon Heterojunction Solar Cells," *Solar Energy Materials and Solar Cells* 265 (2024): 112620, https://doi.org/10.1016/j.solmat.2023.112620.

18. T. Wenzel, A. Lorenz, E. Lohmüller, et al., "Progress With Screen Printed Metallization of Silicon Solar Cells—Towards 20 μm Line Width and 20 mg Silver Laydown for PERC Front Side Contacts," *Solar*

Energy Materials and Solar Cells 244 (2022): 111804, https://doi.org/10.1016/j.solmat.2022.111804.

19. S. Tepner, N. Wengenmeyr, M. Linse, A. Lorenz, M. Pospischil, and F. Clement, "The Link Between Ag-Paste Rheology and Screen-Printed Solar Cell Metallization," *Advanced Materials Technologies* 5, no. 10 (2020): 1–9, https://doi.org/10.1002/admt.202000654.

20. S. Tepner, L. Ney, M. Linse, et al., "Screen Pattern Simulation for an Improved Front-Side Ag-Electrode Metallization of Si-Solar Cells," *Progress in Photovoltaics: Research and Applications* 28, no. 10 (2020): 1054–1062, https://doi.org/10.1002/pip.3313.

21. M. Pospischil, T. Fellmeth, A. Brand, et al., "Optimizing Fine Line Dispensed Contact Grids," *Energy Procedia* 55 (2014): 693–701, https://doi.org/10.1016/j.egypro.2014.08.046.

22. M. Pospischil, T. Riebe, A. Jimenez, et al., "Applications of Parallel Dispensing in PV Metallization," *AIP Conference Proceedings* 2156 (2019): 020005, https://doi.org/10.1063/1.5125870.

23. J. Schube, T. Fellmeth, M. Jahn, R. Keding, and S. W. Glunz, "Advanced Metallization With Low Silver Consumption for Silicon Heterojunction Solar Cells," *AIP Conference Proceedings* 2156 (2019): 020007, https://doi.org/10.1063/1.5125872.

24. K. Gensowski, M. Much, E. Bujnoch, S. Spahn, S. Tepner, and F. Clement, "Filament Stretching During Micro-Extrusion of Silver Pastes Enables an Improved Fine-Line Silicon Solar Cell Metallization," *Scientific Reports* 12, no. 1 (2022): 12318, https://doi.org/10.1038/s41598-022-16249-5.

25. "Conductive Copper Pastes Portfolio Overview," https://copprint.com/wp-content/uploads/2021/04/copprints-product-portfolio-april-2021.pdf.

26. A. Ebong, S. Huneycutt, S. Grempels, K. Ankireddy, R. Dharmadasa, and T. Druffel, "Progress of Atmospheric Screen-Printable Cu Paste for High Efficiency PERC Solar Cells," in *Conference Record of the IEEE Photovoltaic Specialists Conference*, (Institute of Electrical and Electronics Engineers Inc., 2021): 1417–1420, https://doi.org/10.1109/PVSC43889.2021.9518703.

27. S. Grempels, S. Huneycutt, A. Ebong, R. Dharmadasa, K. Ankireddy, and T. Druffel, "Rapid Thermal Annealing of Screen-Printable Atmospheric Cu Pastes for Perc Solar Cell," in *HONET 2020—IEEE 17th International Conference on Smart Communities: Improving Quality of Life Using ICT, IoT and AI*, (Institute of Electrical and Electronics Engineers Inc., 2020): 244–248, https://doi.org/10.1109/HONET50430.2020.9322819.

28. T. Druffel, R. Dharmadasa, K. Ankireddy, K. Elmer, A. Ebong, and S. Huneycutt, "Copper Based Front Side Metalization Contacts Screen Printed and Fired in Air Demonstrating Durability," in *Conf. Rec. IEEE Photovolt. Spec. Conf.* (IEEE, 2020): 2609–2611, https://doi.org/10.1109/PVSC45281.2020.9300763.

29. B. Hallam, M. Kim, Y. Zhang, et al., "The Silver Learning Curve for Photovoltaics and Projected Silver Demand for Net-Zero Emissions by 2050," *Progress in Photovoltaics: Research and Applications* 31, no. 6 (2023): 598–606, https://doi.org/10.1002/pip.3661.

30. Y. Zhang, S. Wang, L. Wang, et al., "Ultra-Lean Silver Screen-Printing for Sustainable Terawatt-Scale Photovoltaic," *Solar RRL* 8, no. 17 (2024): 2400478, https://doi.org/10.1002/solr.202400478.

31. J. Yu, J. Li, Y. Zhao, et al., "Copper Metallization of Electrodes for Silicon Heterojunction Solar Cells: Process, Reliability and Challenges," *Solar Energy Materials and Solar Cells* 224 (2021): 110993, https://doi.org/10.1016/j.solmat.2021.110993.

32. A. Ebong, D. Intal, S. Huneycutt, et al., "Screen Printable Copper Pastes for Silicon Solar Cells," *Solar Energy Materials and Solar Cells* 265 (2024): 112633, https://doi.org/10.1016/j.solmat.2023.112633.

33. A. Lennon, J. Colwell, and K. P. Rodbell, "Challenges Facing Copper-Plated Metallisation for Silicon Photovoltaics: Insights From Integrated Circuit Technology Development," *Progress in Photovoltaics: Research and Applications* 27, no. 1 (2019): 67–97, https://doi.org/10.1002/pip.3062.

34. C. Yu, K. Gao, C. W. Peng, et al., "Industrial-Scale Deposition of Nanocrystalline Silicon Oxide for 26.4%-Efficient Silicon Heterojunction Solar Cells With Copper Electrodes," *Nature Energy* 8 (2023): 1375–1385, https://doi.org/10.1038/s41560-023-01388-4.

35. "Products—Copprint," accessed July 16, 2023, https://www.copprint.com/products/#LF-380.

36. "SunDrive Achieves 26.41% Efficiency With Copper-Based Solar Cell Tech," pv magazine International, accessed July 14, 2023, https://www.pv-magazine.com/2022/09/05/sundrive-achieves-26-41-efficiency-with-copper-based-solar-cell-tech/.

37. J. Haschke, R. Lemerle, B. Aïssa, et al., "Annealing of Silicon Heterojunction Solar Cells: Interplay of Solar Cell and Indium Tin Oxide Properties," *IEEE Journal of Photovoltaics* 9, no. 5 (2019): 1202–1207, https://doi.org/10.1109/JPHOTOV.2019.2924389.

38. "Öffentlicher Abschlussbericht des For-schungsvorhabens "Großflächige, kontaktlose Druckverfahren und Materialen zur Erzeugung feiner Struk-turen für Hocheffiziente Solarzellen" Akronym: "GECKO"."

39. K. Gensowski, M. Palme, I. Langhof, et al., "Paste Development for an Optimized Filament Stretching Effect During Parallel Dispensing on Transparent Conductive Oxide Layers for Solar Cell Metallization," *Advanced Engineering Materials* 25, no. 17 (2023): 1–15, https://doi.org/10.1002/adem.202300010.

40. R. Janoch, A. M. Gabor, A. Anselmo, and C. E. Dube, "Contact Resistance Measurement—Observations on Technique and Test Parameters," in *2015 IEEE 42nd Photovolt. Spec. Conf. PVSC* (IEEE, 2015), https://doi.org/10.1109/PVSC.2015.7355851.

41. S. Zogbo, W. Favre, O. Bonino, and M. E. Gueunier-Farret, "Defining Specifications for Accurate Metal/TCO Specific Contact Resistivity Measurements by TLM in Silicon Heterojunction Devices," *Solar Energy Materials & Solar Cells* 265, no. September 2023 (2024): 112623, https://doi.org/10.1016/j.solmat.2023.112623.

42. "G&G Electronic Balance JJ224BC Analytical Balance 0.1mg - China Electronic Balance and Balance Jj224bc," accessed May 28, 2024, https://www.made-in-china.com/showroom/jingyanggz/product-detailBxZrLuPbagRz/China-G-G-Electronic-Balance-JJ224BC-Analytical-Balance-0-1mg.html.

43. W. Duan, T. Rudolph, H. T. Gebrewold, et al., "Insights Into the Heat-Assisted Intensive Light-Soaking Effect on Silicon Heterojunction Solar Cells," *Solar RRL* 8 (2024): 2400383, https://doi.org/10.1002/solr.202400383.

44. H. Park, Y. J. Lee, J. Park, et al., "Front and Back TCO Research Review of a-Si/c-Si Heterojunction With Intrinsic Thin Layer (HIT) Solar Cell," *Transactions on Electrical and Electronic Materials*. Korean Institute of Electrical and Electronic Material Engineers June 19 (2018): 165–172, https://doi.org/10.1007/s42341-018-0026-8.

45. K. Bothe, C. Kruse, D. Hinken, and R. Brendel, "Contacting of Busbarless Solar Cells for Accurate I-V Measurements," in *37th European Photovoltaic Solar Energy Conference and Exhibition*, vol. 19, No. 5 (AIP Publishing, 2020): 277–281.

46. B. H. Teo, A. Khanna, V. Shanmugam, et al., "Development of Nanoparticle Copper Screen Printing Pastes for Silicon Heterojunction Solar Cells," *Solar Energy* 189 (2019): 179–185, https://doi.org/10.1016/j.solener.2019.07.055.

47. M. Mikolášek, M. Nemec, J. Kováč, et al., "The Influence of Post-Deposition Annealing Upon Amorphous Silicon/Crystalline Silicon Heterojunction Solar Cells," *Materials Science & Engineering, B: Solid-State Materials for Advanced Technology* 189 (2014): 1–6, https://doi.org/10.1016/j.mseb.2014.07.003.

48. X. Li, Y. Xiong, Y. Yang, et al., "Intensive Light Soaking Improves Electricity Generation of Silicon Heterojunction Solar Cells by the

Anomalous Staebler-Wronski Effect," *Applied Physics Express* 15, no. 9 (2022): 091001, https://doi.org/10.35848/1882-0786/ac8784.

49. S. Siraj, S. Tahir, A. Ali, N. Amin, K. Mahmood, and A. Manzoor, "Assessing the Impact of Front Grid Metallization Pattern on the Performance of BSF Silicon Solar Cells," *SILICON* 13, no. 12 (2021): 4237–4245, https://doi.org/10.1007/s12633-021-01235-9.

Appendix A

Figure A1 presents the photovoltaic parameters for SHJ solar cells, including efficiency (η) in (a), open-circuit voltage (Voc) in (b), short-circuit current density (Jsc) in (c), fill factor (FF) in (d), pseudo-fill factor (pFF) in (e), and series resistance (Rs) in (f). The data are shown for cells before sintering (bS), after sintering (aS) at different temperatures (280°C, 320°C, and 360°C) for 5 s, and after light soaking (LiSo). These parameters provide insights into the efficiency variations discussed in the results section. The observed decrease in efficiency with increasing sintering temperature is attributed to the corresponding declines in V_{oc}, J_{sc}, *pFF*, and *FF*. Light soaking, on the other hand, aids in partially recovering these losses, particularly by improving V_{oc}, *pFF*, and *FF*.

Figure A2 presents the photovoltaic parameters for SHJ solar cells, including efficiency (η) in (a), open-circuit voltage (Voc) in (b), short-circuit current density (Jsc) in (c), fill factor (FF) in (d), pseudo-fill factor (pFF) in (e), and series resistance (Rs) in (f). The data are shown for cells before sintering (bS), after sintering (aS) at different times (5, 20, and 40 s) at 300°C and after light soaking (LiSo). These parameters provide insights into the efficiency variations discussed in the results section. The observed decrease in efficiency with increasing sintering temperature is attributed to the corresponding declines in V_{oc}, J_{sc}, *pFF*, and *FF*. Light soaking, on the other hand, aids in partially recovering these losses, particularly by improving V_{oc}, *pFF*, and *FF*.

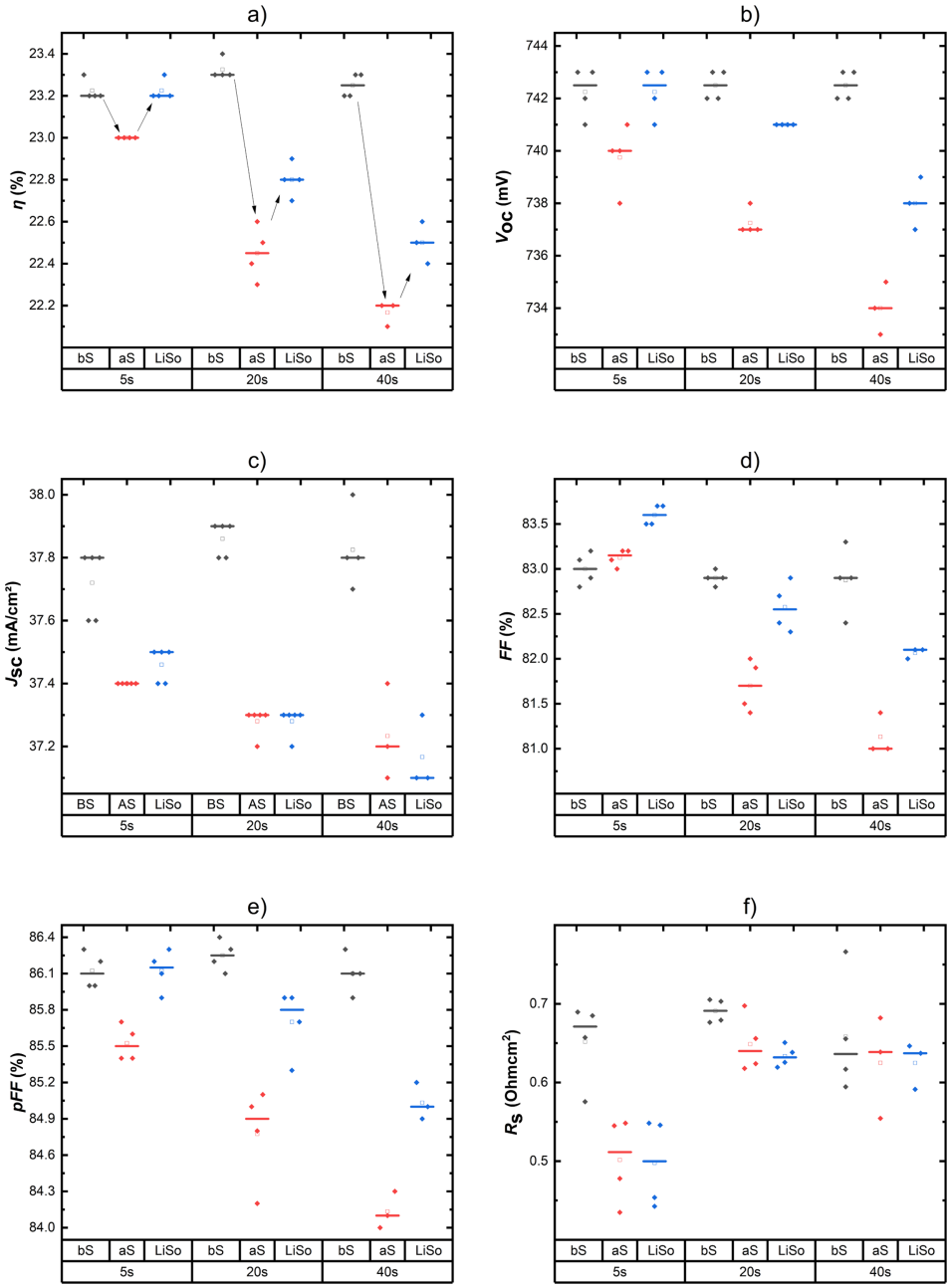

FIGURE A1 | Photovoltaics parameters showing in (a) the efficiencies (η), (b) the open circuit voltages (V_{oc}), (c) the short circuit current densities (J_{sc}), (d) the fill factors (FF), (e) the pseudo-fill factors (pFF), and (f) the series resistances (R_s), for SHJ solar cells before sintering (bS), after sintering (aS) at different temperatures (280°C, 320°C, and 360°C) for 5 s and light soaked (LiSo).

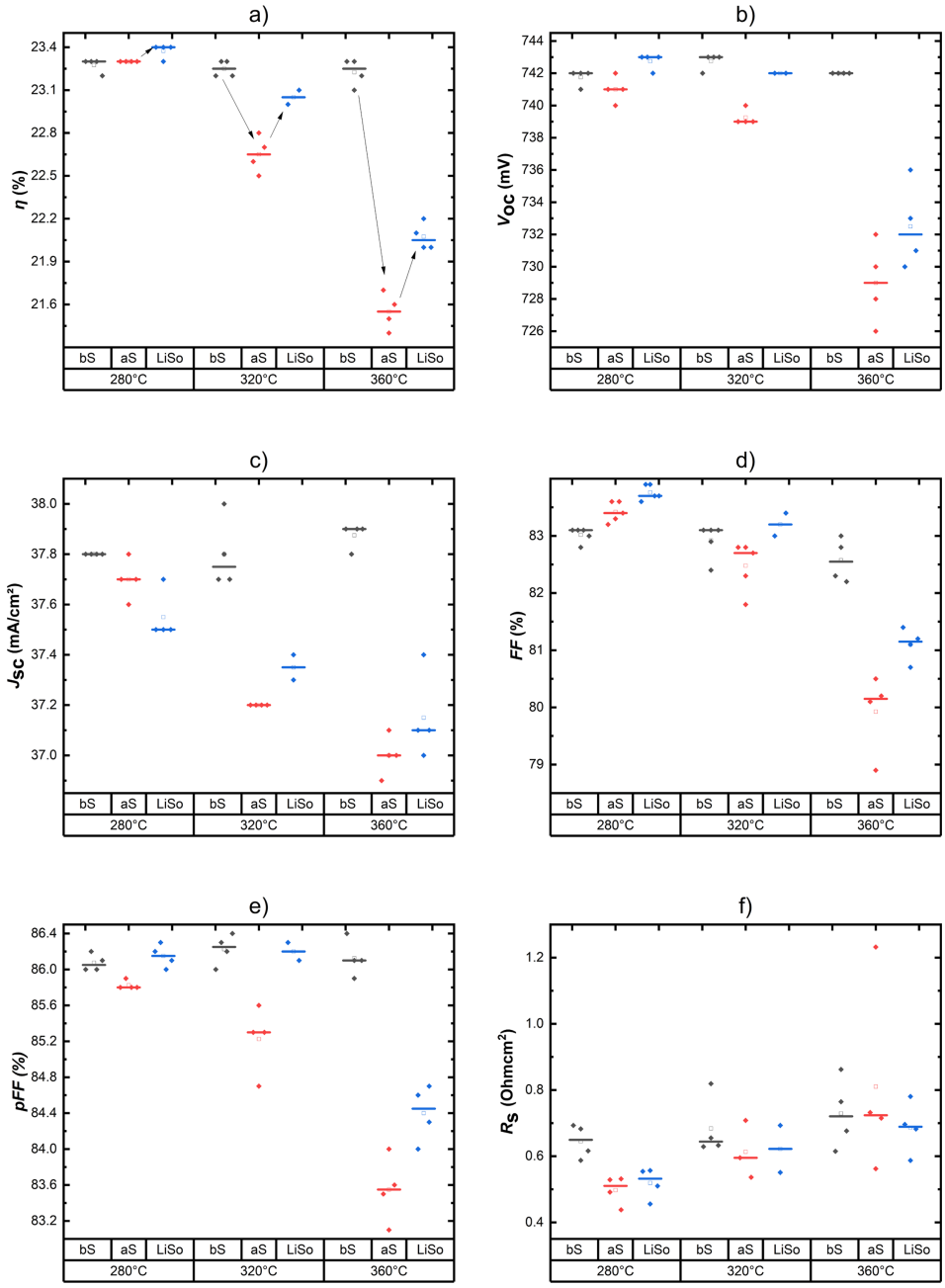

FIGURE A2 | Photovoltaics parameters showing in (a) the efficiencies (η), (b) the open circuit voltages (V_{oc}), (c) the short circuit current densities (J_{sc}), (d) the fill factors (FF), (e) the pseudo-fill factors (pFF), and (f) the series resistances (R_s), of solar cells for different sintering times at 300°C.